Heliyon 5 (2019) e01762

Contents lists available at ScienceDirect

Heliyon

journal homepage: www.heliyon.com

Computational screening of carbon monoxide (CO) adsorption over neutral and charged Al_7 clusters

Z. Abdeveiszadeh, E. Shakerzadeh, S. Noorizadeh *

Chemistry Department, Faculty of Sciences, Shahid Chamran University of Ahvaz, Ahvaz, Iran

ARTICLE INFO

Keywords:
Theoretical chemistry
Physical chemistry
Materials chemistry

ABSTRACT

A density functional theory study on the structures and chemical bonding of charged (Al_7^+ and Al_7^-) and neutral Al_7 clusters is presented. A distorted octahedral structure with an aluminum atom decorating one of the aluminum faces of the octahedron is predicted for these clusters. The AdNDP analysis reveals double (σ- and π-) aromatic and antiaromatic characteristics of Al_7^+ and Al_7^- clusters, respectively. The UV-Vis Spectra of these clusters are also investigated using TD-DFT method. The molecular adsorption of carbon monoxide on the mentioned clusters is also explored. It is found that, the binding of CO through its carbon atom on considered clusters is a physical adsorption and Al_7^- cluster shows the most tendency for the CO adsorption. The NBO analysis and density of states spectra confirm the weak interaction between carbon atom of CO and the aluminum atom of these clusters.

1. Introduction

Clusters are defined as an assembly of molecules or atoms that are weakly bound together and display properties, intermediate between those of isolated gas-phase molecules and bulk solid. Therefore, they allow one to study how physical and chemical properties change in transition from an isolated molecule to a condensed phase. Interest in small metallic clusters has grown dramatically in the past few decades [1, 2, 3, 4, 5, 6, 7, 8] and since aluminum is a common and cheap metal, its clusters are probably the most studied systems among the other metallic clusters [9, 10, 11, 12, 13]. Atomic clusters that exhibit some properties of elemental atoms are called superatoms. Certain aluminum clusters show superatom properties. For example, Al_7 is known as superatom and its potential to construct excellent non-linear optical materials has been investigated [14]. Anionic Al clusters (Al_n^- with n = 1, 2, 3, …) also have superatomic properties [15, 16]. The properties of atomic clusters depend on cluster size. Different studies show that the binding energies of Al clusters increase monotonically with size, but some of them, such as Al_7^+ and Al_{13}^- are more stable than their neighbors [10, 12]. The enhanced stability of these clusters can be accounted for by the electronic shell approach of jellium model [17, 18]; in which, clusters with 2, 8, 20, 40, … electrons that have close electronic shell show more stability and are known as magic clusters [19]. Therefore, Al_7^+ and Al_{13}^- clusters with 20 and 40 valence electrons, respectively, according to jellium model are two examples of magic clusters [10, 12].

During the past few decades, density functional theory (DFT) has been frequently used to study a wide variety of properties of metal clusters [12, 20, 21, 22, 23, 24, 25, 26, 27, 28, 29, 30]. Interaction of clusters with different atoms or molecules is the interesting topic in cluster science, which investigates the stability and catalytic properties of clusters. It is shown that, these interactions are influenced by the size of cluster. For instance, Upton and coworkers [31] showed that smallest aluminum cluster could adsorb H_2 molecule is Al_6 and for clusters containing more than 6 atoms, the reactivity decrease rapidly with increasing the cluster size. The interaction of hydrogen molecule with neutral and charged $Al_{12}X$ clusters (X = Mg, Al, Si) was investigated and obtained results indicate that this adsorption is dissociative chemisorption [32]. Mohamed Maatallah and coworkers [33] studied bare and hydrogenated Al_n (n = 5–7) clusters to evaluate the ability of storing molecular hydrogen. Dissociative adsorption of deuterium molecule (D_2) on the neutral and anionic Al_n Al_n(n = 1–9) clusters has also been investigated [34].

Since the presence of toxic gases in environment affects human health, production of a sensor or a device able to detect or adsorb pollutant gases and remove them from the air is important. The adsorption of carbon monoxide on metal surfaces is probably one of the most studied systems in surface science [35, 36, 37, 38, 39]. The interaction of the lone pair ligands, such as CO, with one metal atom leads, very often, to a repulsive potential curve [40]; which is largely due to the repulsion between the metal valence electron(s) and the ligand lone pair.

* Corresponding author.
E-mail address: noorizadeh_s@scu.ac.ir (S. Noorizadeh).

https://doi.org/10.1016/j.heliyon.2019.e01762
Received 22 December 2018; Received in revised form 12 April 2019; Accepted 15 May 2019

Table 1
Total energies included zero-point correction (E), HOMO and LUMO energies (E_H and E_L) and HOMO-LUMO gaps (HL gap) in a.u. using B3LYP/6-311G* and Cam-B3LYP/6-311G* [values in bracket] methods.

Cluster	Multiplicity	E	E_H	E_L	HL gap
Al_7^-	1	-1697.2218	-0.0358	0.0228	0.0586
	3	[-1697.0553]	[-0.0708]	[0.0562]	[0.1270]
		-1697.2171	-0.0261	0.0212	0.0473
Al_7^+	1	-1696.9389	-0.3443	-0.2463	0.0980
	3	[-1696.7722]	[-0.3797]	[-0.2088]	[0.1709]
		-1696.9003	-0.3110	-0.2532	0.0578
Al_7	2	-1697.1482	-0.1695	-0.1077	0.0618
	4	[-1696.9842]	[-0.2107]	[-0.0737]	[0.1370]
		-1697.1173	-0.1701	-0.1121	0.0580

If, however, the cluster contains four or five metal atoms chosen to represent the first two layers of a single crystal surface, the interaction energy is in reasonable agreement with the chemisorption energy of the ligand on a metal surface [41].

The structure and temperature of surface can influence the adsorption nature. Adsorption of CO on some metal clusters such as Na, Ca and Ti leads to dissociation of carbon monoxide to carbon and oxygen atoms and forming the C-Metal and O-Metal bonds. On the other hand, for some d-block metals such as Cu and Ag the carbon monoxide remains in molecular form after adsorption. Since the formed Metal-CO bond is weak, it is possible that Metal-CO bond is broken and CO desorbed from the surface by increasing the temperature of surface.

Although the chemistry of superatom draws a great deal of attention, research on the potential applications of superatom compounds is rare. In this article, the adsorption of CO molecule on Al_7^-, Al_7^+ and Al_7 clusters are investigated. Also, Density of States (DOS), Natural Bond Orbital (NBO) and Adaptive Natural Density Partitioning (AdNDP) analysis as well as UV-Vis spectra of these clusters are investigated. We hope this study could extend the field of superatom chemistry.

2. Calculation

All calculations are performed without symmetry constraints using both B3LYP and CAM-B3LYP methods with 6-311G* basis set, as implemented in Gaussian 09 suite of program [42]. These levels of theory have been used to investigate of different properties of nanocages [43, 44, 45] and various aluminum systems [46, 47, 48] in several studies. Therefore, it seems these methods are reliable for study of the considered systems.

The adsorption energy (E_{ads}) due to the interaction of CO molecule with the mentioned clusters (Al_7, Al_7^+ and Al_7^-) is calculated as:

$$E_{ads} = E_{cluster-co} - (E_{cluster} + E_{co}) \quad (1)$$

where$E_{cluster-co}$ denotes the total energy of CO-adsorbed system and $E_{cluster}$ and E_{CO} are the total energies of free cluster and CO molecule, respectively. The negative adsorption energy indicates an exoergic pro-

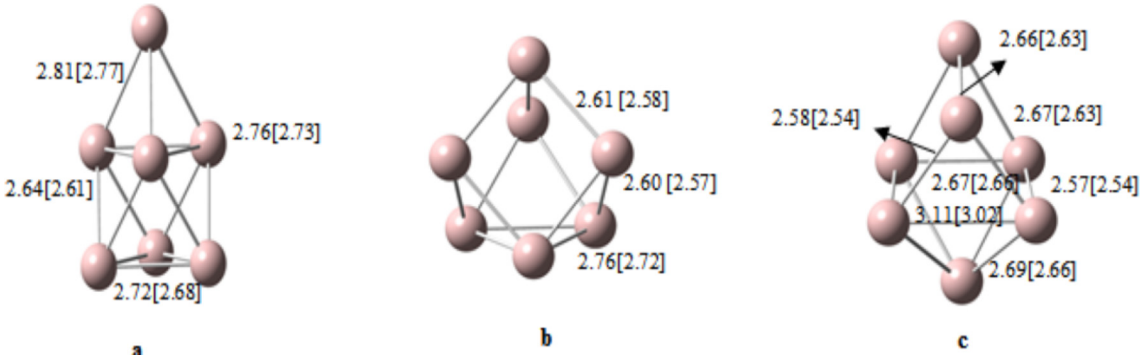

Fig. 1. Optimized structures as well as calculated bond lengths (in Å) of a) Al_7^-,b) $Al_7^+$and c) Al_7 clusters at B3LYP/6-311G* and CAM-B3LYP/6-311G* [values in bracket].

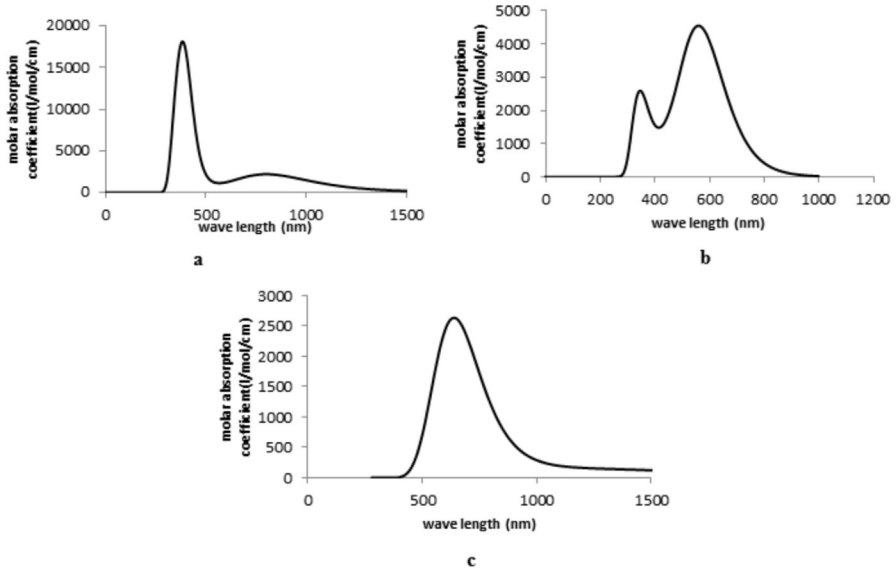

Fig. 2. UV-Visible spectra of a) Al_7^-, b) Al_7^+, c) Al_7 clusters.

Table 2
Excitation energies (eV), wavelengths (nm), oscillator strengths and maximum transitions for Al_7^- at TDDFT/Cam-B3LYP/6-311+G* method.

Excitation	E(eV)	$\lambda(nm)$	f	Maximum Transition
$S_0 \rightarrow S_4$	1.3169	941.48	0.010	H→L+1(90.2%)
$S_0 \rightarrow S_5$	1.4359	863.49	0.014	H-1'→L' (44.4%) H-1→L (44.4%)
$S_0 \rightarrow S_6$	1.4359	863.49	0.014	H-1'→L(44.4%) H-1→L' (44.4%)
$S_0 \rightarrow S_{25}$	3.1097	398.70	0.278	H→L+3(73.7%)
$S_0 \rightarrow S_{26}$	3.1594	392.43	0.027	H-3→L+1(31.3%) H-1→L+6(24.3%)
$S_0 \rightarrow S_{27}$	3.1594	392.43	0.027	H-3'→L+1(31.3%) H-1'→L+6(24.3%)
$S_0 \rightarrow S_{30}$	3.5187	352.36	0.201	H-1'→L+5 (18.88%) H-1→L+2′(10.1%)

cess, and therefore a species with a more negative E_{ads} value is more favorable thermodynamically. Note that, the adsorption energy encompasses both binding (E_{bin}) and deformation (E_{def}) energy contributions occurred during the adsorption process. Since the obtained deformation energies are not negligible for some of the studied systems, they are considered in this study. Therefore, the following definitions are applied to separate these contributions from each other:

$$E_{bin} = E_{cluster-co} - \left(E^{sp}_{cluster} + E^{sp}_{co}\right) \quad (2)$$

$$E = \left(E^{sp}_{cluster} - E_{cluster}\right) + \left(E^{sp}_{co} - E_{co}\right) = E_{ads} - E_{bin} \quad (3)$$

where $E^{sp}_{cluster}$ and E^{sp}_{co} are the total single point energies of cluster and CO in their relaxed complex geometries. All energies are corrected through basis set superposition error (BSSE) using the counterpoise method [49].

The charge transfer is also investigated using both Natural Bond Orbital (NBO) scheme and Electron Density Difference (EDD) maps. EDD is expressed as:

$$\nabla\rho = \rho_{Cluster-CO} - (\rho_{CO} + \rho_{Cluster}) \quad (4)$$

where $\rho_{Cluster-CO}$ is the electron density of the total CO + Al_7 complex, and ρ_{CO} as well as $\rho_{Cluster}$ are the unperturbed electron densities of the carbon monoxide and aluminum cluster, respectively.

The changes in electronic structures of aluminum clusters are

Table 3
Excitation energies (eV), wavelengths (nm), oscillator strengths and maximum transitions for Al_7^+ at TDDFT/Cam-B3LYP/6-311+G* method.

Excitation	E(eV)	$\lambda(nm)$	f	Maximum transition
$S_0 \rightarrow S_1$	2.1163	585.85	0.029	H→L+1(66.9%)
$S_0 \rightarrow S_2$	2.1163	585.85	0.029	H→L+1′(66.9%)
$S_0 \rightarrow S_4$	2.1768	569.58	0.013	H→L(83.6%)
$S_0 \rightarrow S_7$	2.3112	536.45	0.026	H→L+2(75.6%)
$S_0 \rightarrow S_{13}$	2.7669	448.09	0.010	H→L+3′(78.3%)
$S_0 \rightarrow S_{14}$	2.7669	448.09	0.010	H→L+3(78.3%)
$S_0 \rightarrow S_{22}$	3.3143	374.09	0.020	H-2→L(81.8%)
$S_0 \rightarrow S_{29}$	3.6990	335.18	0.022	H-3'→L+2(59.6%) H-2→L+3′(12.6%)
$S_0 \rightarrow S_{30}$	3.6990	335.18	0.022	H-3→L+2(59.6%) H-2→L+3(12.6%)

Table 4
Excitation energies (eV), wavelengths (nm), oscillator strengths and maximum transitions for Al_7 at TDDFT/Cam-B3LYP/6-311+G* method.

Excitation	E(eV)	$\lambda(nm)$	f	Maximum transition
$D_0 \rightarrow D_{16}$	1.8891	656.32	0.022	H(β)→L+2(β) (47.8%) H-1(α)→L(α) (21.6%)
$D_0 \rightarrow D_{17}$	1.9435	637.94	0.016	H-1(α)→L+1(α) (45.3%) H(β)→L+1(β) (17.5%)

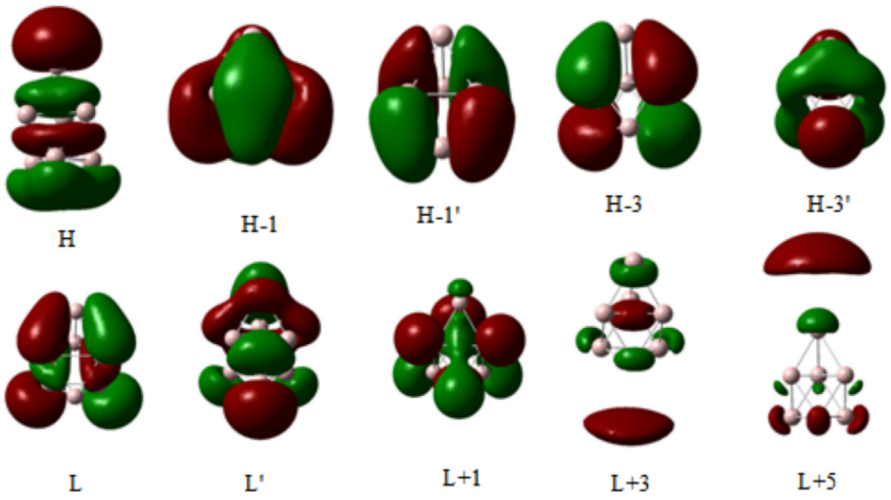

Fig. 3. Frontier molecular orbitals involved in the crucial excitations for Al_7^- Cluster.

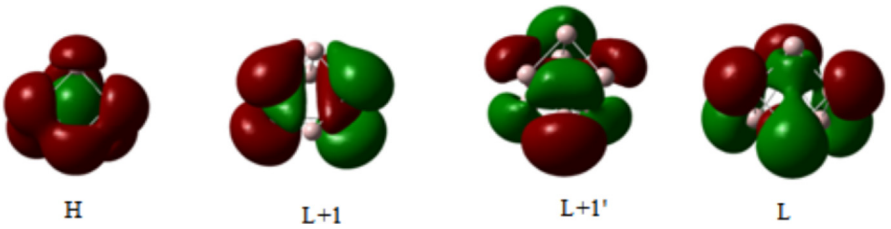

Fig. 4. Frontier molecular orbitals involved in the crucial excitations for Al_7^+ Cluster.

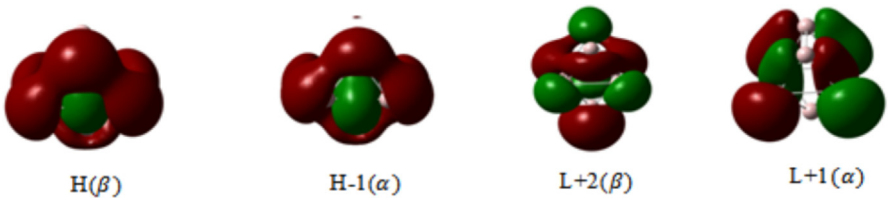

Fig. 5. Frontier molecular orbitals involved in the crucial excitations for Al_7 Cluster.

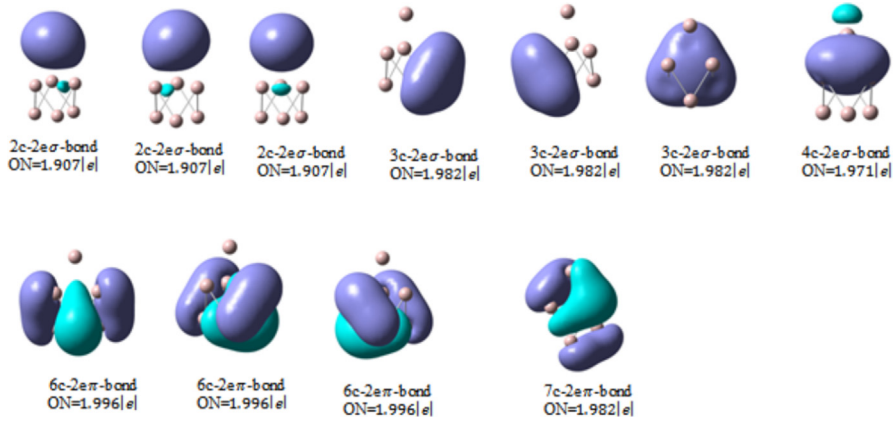

Fig. 6. Chemical bonding analysis of Al_7^- cluster using the AdNDP method. ON stands for occupation number (residual electron = 0.4e) (isovalue = 0.02a.u.) (σ-antiaromatic and π-antiaromatic).

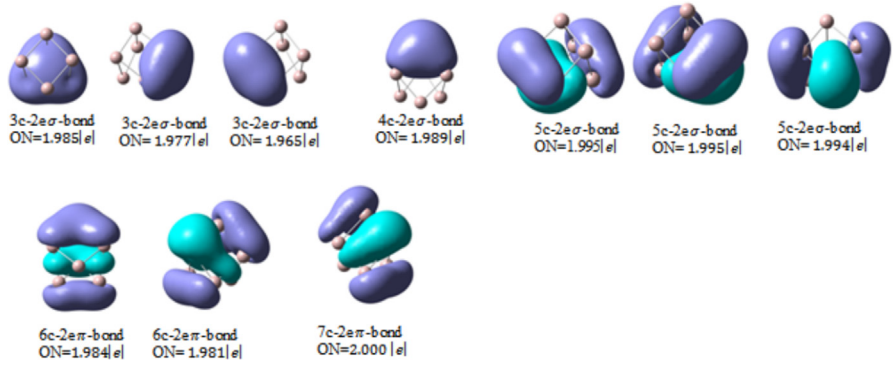

Fig. 7. Chemical bonding analysis of Al_7^+ cluster using the AdNDP method. ON stands for occupation number (residual electron = 0.16e) (isovalue = 0.02a.u.) (σ-aromatic and π-aromatic).

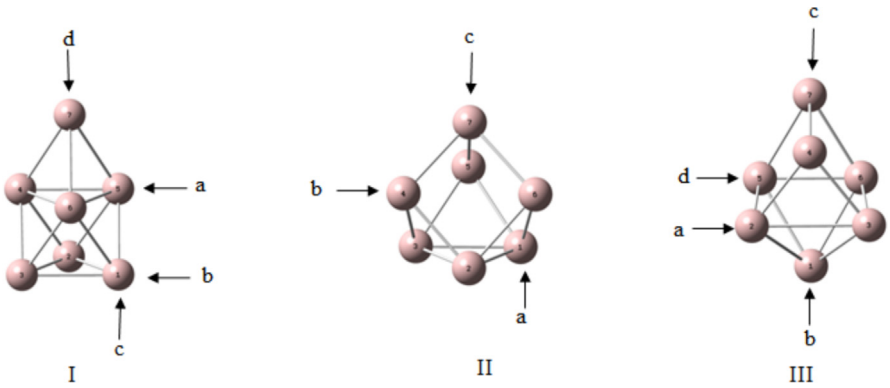

Fig. 8. Different sites (a, b, c and d) that considered for the adsorption of CO molecule on **I**)Al_7^-, **II**)Al_7^+ and **III**)Al_7 clusters.

evaluated through Frontier Molecular Orbitals (FMO); i.e. HOMO-LUMO (H-L) gap. The AdNDP analysis, density of states (DOS) and Partial Density of States (PDOS) are also evaluated using Multiwfn 3.3.9 software [50].

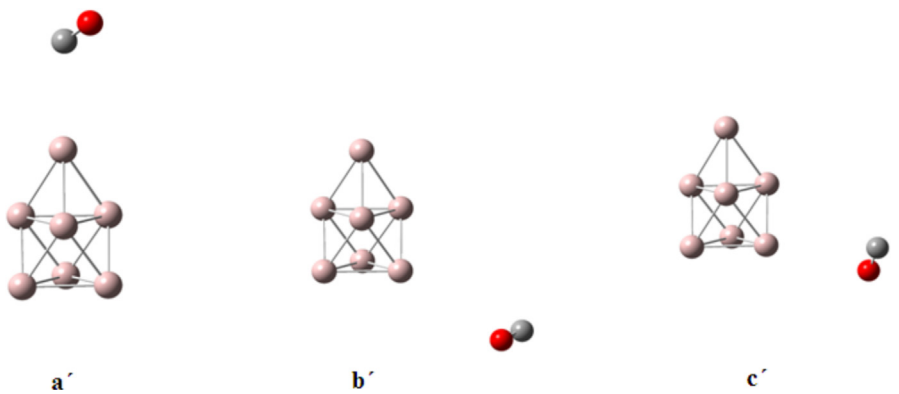

Fig. 9. Optimized structures of Al_7^-CO complexes in which oxygen atom of CO approaches to Al_7^- from a') top, b') below, c') below-beside and d') top-beside.

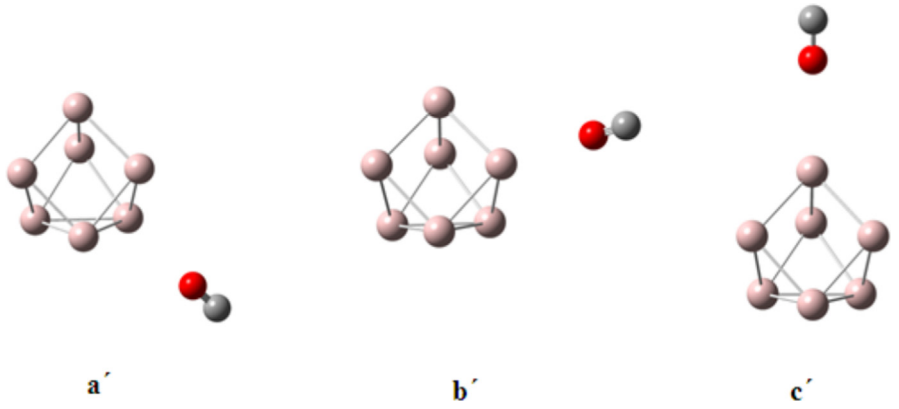

Fig. 10. Optimized structures of Al_7^+CO complexes in which oxygen atom of CO approaches to $Al_7^+$from a') below, b') beside and c')top.

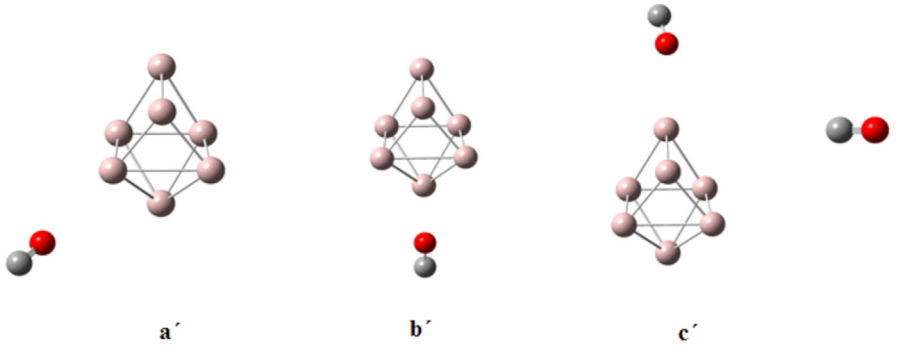

Fig. 11. Optimized structures of Al_7CO complexes in which oxygen atom of CO approaches to Al_7 from a') below-beside, b') below, c') top and d') top-beside.

Table 5
The obtained basisset superposition errors (δ_{BSSE}), deformation (E_{def}), corrected binding (E_{bin}^{corr}), and adsorption energies (E_{ads}^{corr}) for the binding of CO through itsoxygen atom to Al_7-(all in eV) using B3LYP/6-311G* and Cam-B3LYP/6-311G* [values in bracket)] methods.

Configuration	δ_{BSSE}	E_{def}	E_{bin}^{corr}	E_{ads}^{corr}
a′	0.0222	0.0011	-0.0167	-0.0156
	[0.0331]	[0.0004]	[-0.0062]	[-0.0058]
b′	0.0249	0.0004	0.0008	0.0012
	[0.0287]	[0.0003]	[0.0001]	[0.0004]
c′	0.0248	0.0003	-0.0003	0.0000
	[0.0331]	[0.0001]	[-0.0082]	[-0.0081]
d′	0.0222	0.0008	-0.0174	-0.0166
	[0.0331]	[0.0002]	[-0.0060]	[-0.0058]

Table 6
The obtained basis set superposition errors (δ_{BSSE}), deformation (E_{def}), corrected binding (E_{bin}^{corr}), and adsorption energies (E_{ads}^{corr}) for the binding of CO through itsoxygen atom to Al_7^+ (all in eV) using B3LYP/6-311G* and Cam-B3LYP/6-311G* [values in bracket] methods.

Configuration	δ_{BSSE}	E_{def}	E_{bin}^{corr}	E_{ads}^{corr}
a′	0.0537	0.0024	-0.0348	-0.0325
	[0.0613]	[0.0033]	[-0.0556]	[-0.0522]
b′	0.0532	0.0029	-0.0349	-0.0320
	[0.0607]	[0.0049]	[-0.0549]	[-0.0500]
c′	0.0509	0.0036	-0.0434	-0.0399
	[0.0575]	[0.0052]	[-0.0708]	[-0.0655]

Time-dependent density functional theory (TD-DFT) is used to predict

Table 7
The obtained basis set superposition errors (δ_{BSSE}), deformation (E_{def}), corrected binding (E_{bin}^{corr}), and adsorption energies (E_{ads}^{corr}) for the binding of CO through itsoxygen atom to Al_7 (all in eV) using B3LYP/6-311G* and Cam-B3LYP/6-311G* [values in bracket] methods.

Configuration	δ_{BSSE}	E_{def}	E_{bin}^{corr}	E_{ads}^{corr}
a′	0.0364	0.0002	0.0033	0.0035
	[0.0425]	[0.0003]	[-0.0029]	[-0.0027]
b′	0.0319	0.0000	0.0063	0.0064
	[0.0426]	[0.0003]	[-0.0028]	[-0.0025]
c′	0.0291	0.0001	0.0062	0.0063
	[0.0345]	[0.0000]	[0.0045]	[0.0046]
d′	0.0360	0.0001	0.0049	0.0051
	[0.0429]	[0.0002]	[0.0011]	[0.0014]

the UV-Vis absorption spectra of the considered clusters using CAM-B3LYP/6-311+G* level of theory. Note that, diffuse and polarized orbitals, which are necessary for a reliable TD calculation, are included in this basis set. Different numbers of excited states are checked and finally thirty lowest singlet (for Al_7^+ and Al_7^-) and doublet (for Al_7) excited states have been considered for these calculations.

3. Results and discussion

A) Geometrical structures

The initial structures for geometry optimization of Al_7^-, Al_7^+ and Al_7 clusters are given from Li *et.al.* study [11]. Different spin multiplicities are considered for the mentioned neutral (doublet and quartet) and charged (singlet and triplet) clusters for the geometry optimization. It is found that smaller multiplicity causes more stability in all cases (see Table 1). Therefore, just singlet and doublet multiplicities are selected for the charged and neutral clusters, respectively. The stability of the mentioned clusters is confirmed with the vibrational frequency analysis. The absence of imaginary frequencies indicates that the obtained structures are minimum on the potential energy surface.

The obtained stable structures for Al_7^-, $Al_7^+$and Al_7 clusters optimized at B3LYP/6-311G* and CAM-B3LYP/6-311G* levels of theory are shown in Fig. 1. The evaluated bond lengths for these clusters are also given in this figure. Both computational methods predict the same stable geometries for the considered clusters. The considered Al clusters have octahedral structures with an aluminum atom decorating one of the aluminum faces of the octahedron. The presence of the capped aluminum atom causes a distortion in the Al_6 octahedron skeleton. The most deviation from O_h symmetry is observed for neutral Al_7 (with Cs symmetry point group) and the less distortion is observed for charged clusters (with C_3v symmetry point group). These findings are in agreement with the previously report [11]. It is clear that the evaluated bond lengths using CAM-B3LYP method are slightly shorter than those calculated by B3LYP method. The attractive nature of long-range interactions considered in CAM-B3LYP method is responsible for this observation. The evaluated average bond lengths using B3LYP for Al_7^-, Al_7 and Al_7^+ are 2.72 Å, 2.70 Å and 2.66 Å, respectively, imply to more stability of Al_7^+ with respect to the other considered clusters. On the other hand, according to the obtained HOMO-LUMO energy gaps (H-L gaps; a measure of hardness) and based on the Maximum Hardness Principle (MHP) [51], the Al_7^+ species with the most hardness (H-L = 2.6667eV) should be more stable than Al_7 (H-L = 1.6817eV) and Al_7^- (H-L = 1.5946eV) clusters. All of these findings are

Table 8
The obtained basis set superposition errors (δ_{BSSE}), deformation (E_{def}), corrected binding (E_{bin}^{corr}), and adsorption energies (E_{ads}^{corr}) as well as H-L gaps for the considered configurations of Al_7−(all in eV) using B3LYP/6-311G* and Cam-B3LYP/6-311G* [values in bracket] methods.

Configuration	δ_{BSSE}	E_{def}	E_{bin}^{corr}	E_{ads}^{corr}	H-L gap
a	0.0784	0.2927	-0.2545	0.0382	1.6539
	[0.0857]	[0.3100]	[-0.1766]	[0.1334]	[3.5173]
b	0.0818	0.5904	-0.9375	**-0.3471**	1.7295
	[0.0890]	[0.6559]	[-0.8999]	**[-0.2440]**	[3.5494]
c	0.0818	0.5902	-0.9372	**-0.3470**	1.7304
	[0.0890]	[0.6558]	[-0.8997]	**[-0.2440]**	[3.5494]
d	0.0818	0.5906	-0.9377	**-0.3471**	1.7300
	[0.0890]	[0.6555]	[-0.8995]	**[-0.2440]**	[3.5494]

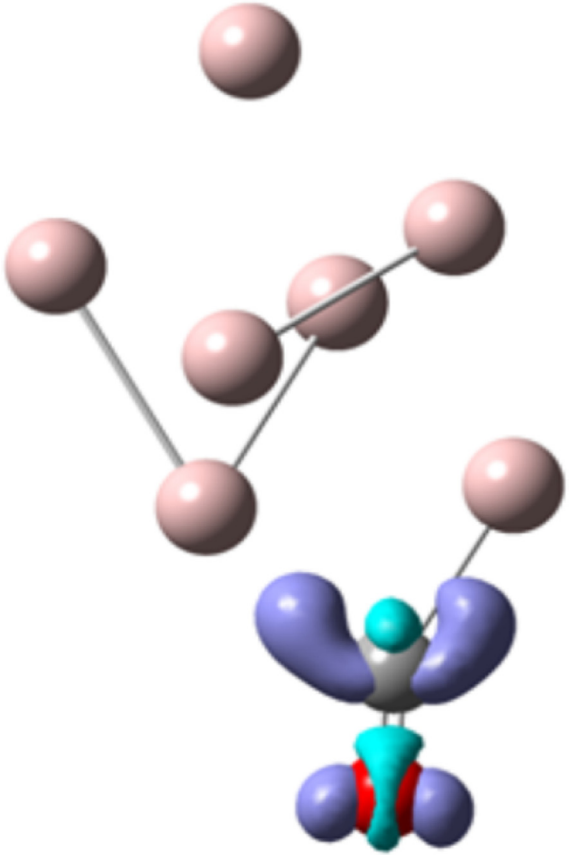

Fig. 13. Difference of electron density of Al_7^-CO (**c** configuration). The blue and green isosurfaces represent the region in which electron density is increased and decreased, respectively after CO binds to Al_7^- (isovalue = 0.01a.u.).

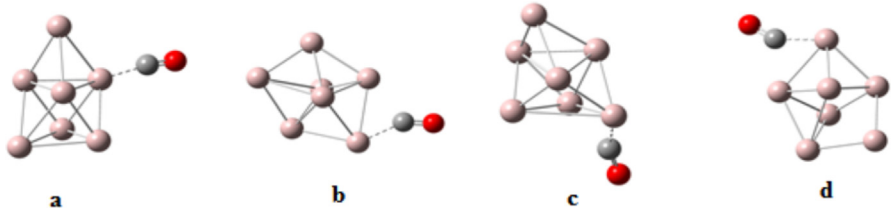

Fig. 12. Optimized structures of Al_7^-CO complexes in which carbon atom of CO approach to Al_7^- from a) top-beside, b) below-beside, c) below and d) top.

Table 9
Natural charge population of the Al_7^-CO complex by B3LYP/6-311G* method. The charge values of Al atoms that are bonded to CO are bolded.

	Al1	Al2	Al3	Al4	Al5	Al6	Al7	C	O
Al_7^-	-0.106	-0.106	-0.106	-0.212	-0.212	-0.212	-0.046		
a	-0.103	-0.103	-0.009	-0.149	**-0.468**	-0.149	0.015	0.400	-0.434
b	**0.232**	0.000	-0.006	-0.130	-0.290	-0.263	0.040	-0.071	-0.512
c	**0.231**	-0.263	-0.290	0.040	-0.005	-0.001	-0.129	-0.071	-0.512
d	0.040	-0.007	-0.129	0.001	-0.261	-0.291	**0.232**	-0.071	-0.512

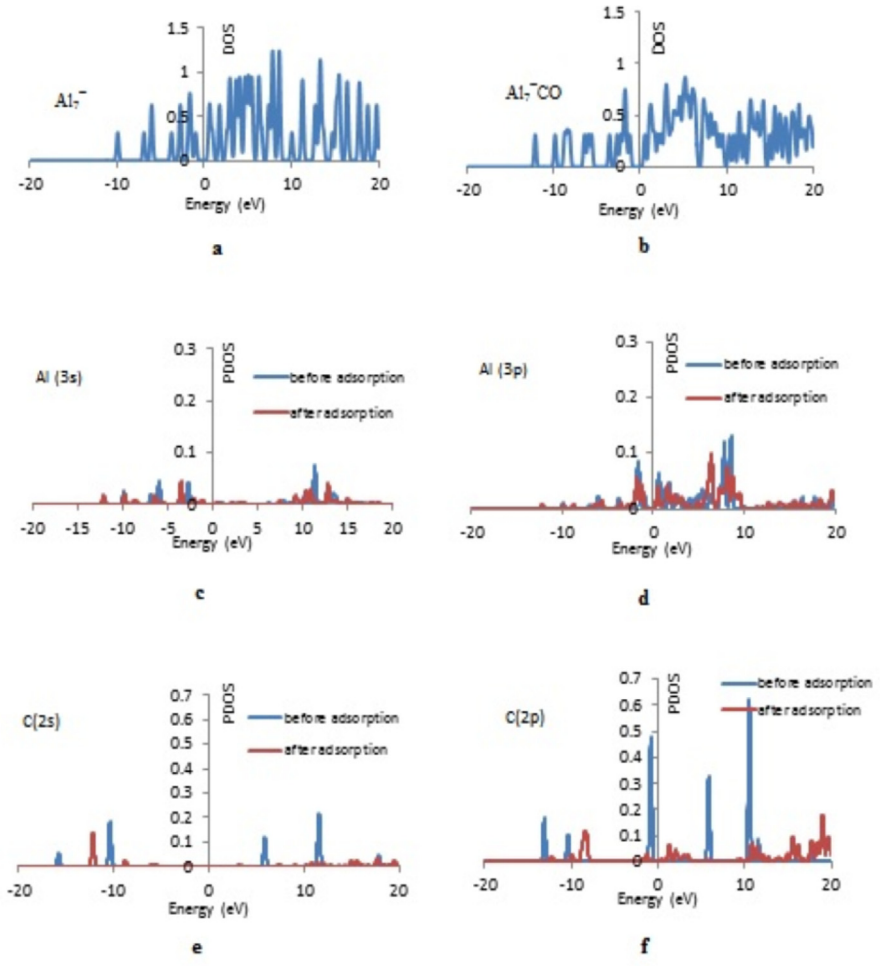

Fig. 14. Total DOS (TDOS) of a) Al_7^- cluster, b) Al_7CO complex (c configuration) as well as Partial DOS (PDOS) of c) 3s and d) 3p valence orbitals of Al atom and e) 2s and f) 2p valence orbitals of carbon atom, before and after adsorption.

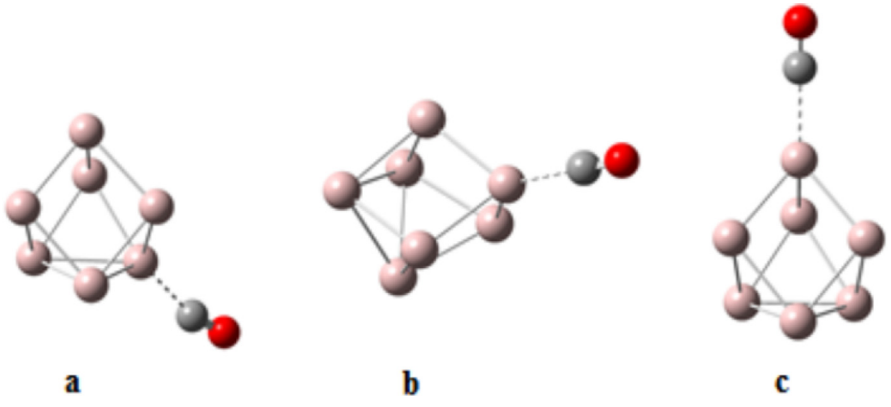

Fig. 15. Optimized structures of Al_7^+CO complexes in which carbon atom of CO approach to Al_7^+ from a) below, b) beside, c) top.

Table 10
The obtained basis set superposition errors (δ_{BSSE}), deformation (E_{def}), corrected binding (E_{bin}^{corr}), and adsorption energies (E_{ads}^{corr}) as well as H-L gaps for the considered configurations of Al_7^+ (all in eV) using B3LYP/6-311G* and Cam-B3LYP/6-311G* [values in bracket] methods.

Configuration	δ_{BSSE}	E_{def}	E_{bin}^{corr}	E_{ads}^{corr}	H-L gap
a	0.0697	0.0403	-0.1490	-0.1087	2.2174
	[0.0756]	[0.0499]	[-0.2094]	[-0.1595]	[4.2613]
b	0.0537	0.0555	-0.2009	**-0.1455**	2.3519
	[0.0539]	[0.0524]	[-0.2593]	**[-0.2068]**	[4.4523]
c	0.0518	0.0549	-0.2008	**-0.1459**	2.3535
	[0.0540]	[0.0528]	[-0.2594]	**[-0.2066]**	[4.4521]

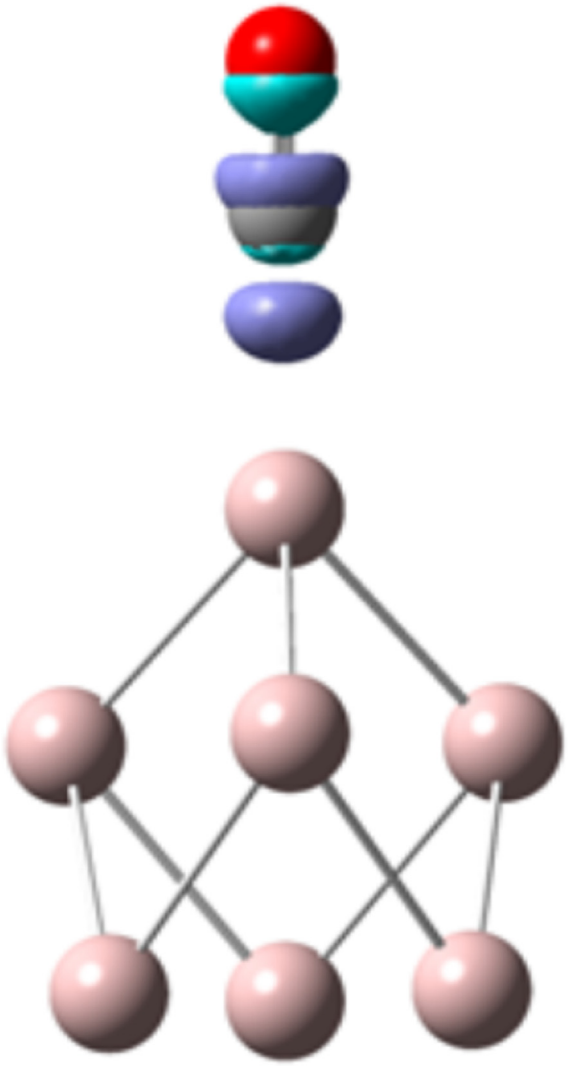

Fig. 16. Difference of electron density of Al_7^+CO (**c** configuration). The blue and green isosurfaces represent the region in which electron density is increased and decreased, respectively after CO binds to Al_7^+ (isovalue = 0.005a.u.).

in accordance with the jellium model, which suggests that the Al_7 cluster with electronic configuration of $1s^2\ 1p^6\ 1d^{10}\ 2s^2\ 2p^1$ prefers to lose the 2p electron to satisfy the magic electron number of 20. Then, it is easy to anticipate that Al_7 is a suitable excess electron donor. It should be mentioned that, the clusters with smaller multiplicities show lower energy and larger H-L gap (see Table 1); which according to the MHP reveals the stability of these multiplicities. This stability should be also due to the aromaticity of Al_7^+ cluster; which will be discussed later.

B) **UV-Vis Spectrum**

The obtained UV-Vis spectra of the Al_7^-, Al_7^+ and Al_7 clusters using TD-DFT calculations, are shown in Fig. 2. The corresponding UV-V is spectrum of Al_7^- (see panel **a** in Fig. 2) consists of two peaks; a nearly sharp peak at about 395 nm and a broad band around 801 nm. Those excited states which have more contributions in these absorption bands are given in Table 2. Transitions from electronic ground state (S_0) to S_{25} and S_{30} excited states show more contributions (with considerable oscillator strength; *f*) in the 395 nm absorption band; and the dominating excitations are H→L+3 and H-1'→L+5 transitions, respectively. On the other hand, transitions to S_4, S_5 and S_6 excited states have more contributions in the broad band at 801 nm. The S_0→S_4 excitationis dominated by H→L+1 transition; whereas H-1'→L′ and H-1'→L transitions have more contributions in excitations from S_0 to degenerate S_5 and S_6 excited states. The molecular orbitals in crucial excitations are depicted in Fig. 3.

The UV-Vis spectrum of Al_7^+ shows two peaks at 345 nm and 558 nm. The excited states with more contributions in these absorption bands are given in Table 3. Excitation from electronic ground state to degenerate S_{29} and S_{30} excited states that have the same oscillator strength ($f = 0.022$) as well as S_{22} excited state have more contributions in the 345 nm adsorption band ($f = 0.020$). Degenerate first and second excited states (S_1 and S_2) as well as S_7 excited state have more contributions in the bands at about 558 nm. The S_0→S_1 and S_0→S_2 transitions are more contributed (%66.9) from H to degenerate L+1 and L+1′ molecular orbitals, respectively. Fig. 4 shows the main orbitals (H, L+1 and L+1′) that in which are contributed the vertical electronic transition in Al_7^+ cluster. Note that, L+1 and L+1′ orbitals are centered on the octahedron aluminum atoms but not on the capped Al atom. Therefore, these transitions decrease the electron density of the capped aluminum atom.

The UV-Vis spectrum of Al_7 shows a nearly broad peak at about 639 nm. According to the reported results in Table 4, transitions from the electronic ground state (D_0) to D_{16} and D_{17} excited states have more contributions (more oscillator strength; *f*) in this peak. These transitions are significantly due to H(β→L+2(β and H-1(α→L+1(α) electron transfers. The majority of H(β and L+2(βelectron densities (see Fig. 5) are lying on the octahedron aluminum atoms and the capped Al atom, respectively. Therefore, this transition causes an electron transfer from peripheral bonding of Oh atoms to the capped aluminum atom. But in H-1(α→L+1(α) transition, the electrons are moved to the Al–Al bonds of the cluster.

C) **AdNDP analysis**

Atomic clusters, in general, are stabilized through non-classical chemical bonding patterns. Therefore, some concepts such as aromaticity are frequently used to describe the stability and structure of a given metallic cluster [52]. To better understand the chemical bonding in the considered aluminum clusters, electron localization analysis using the Adaptive Natural Density Partitioning (AdNDP) is carried out. In fact, AdNDP is a theoretical tool to characterize the chemical bonding [53], and does not depend significantly on the method or basis set [54]. In this approach, the electronic structure of system represents in terms of nc-2e orbitals, in which n can vary from one to the total number of atoms in the corresponding system. It should be mentioned that, nc-2e orbitals with $n > 2$ are associated with the concept of delocalization and therefore aromaticity of the system. Hence, the AdNDP approach is used to anticipate the aromaticity of the considered Al_7^- and Al_7^+ clusters. It should be recalled that, both Al_7^+ and Al_7 have closed-shell electronic structures and AdNDP analysis could be performed appropriately; whereas for neutral Al_7 cluster with odd number of electrons the AdNDP calculations may led to unreliable results. Therefore, this approach is not considered for Al_7 cluster. The results are depicted in Figs. 6 and 7.

Fig. 6 represents the results of the AdNDP analysis for Al_7^- at B3LYP/6-311G* level of theory. This partitioning suggests that σ-bonding in Al_7^- cluster is composed of three 2c-2e localized σ-bonds and four delocalized

Table 11
Natural charge population of the Al_7^+CO complex by B3LYP/6-311G* method. The charge values of Al atoms that are bonded to CO are bolded.

	Al1	Al2	Al3	Al4	Al5	Al6	Al7	C	O
Al_7^+	0.132	0.132	0.132	0.154	0.154	0.154	0.140		
a	**-0.153**	0.162	0.163	0.114	0.145	0.145	0.191	0.549	-0.317
b	0.145	0.154	0.152	**-0.145**	0.143	0.144	0.154	0.564	-0.3115
c	0.143	0.143	0.145	0.154	0.153	0.154	**-0.145**	0.564	-0.311

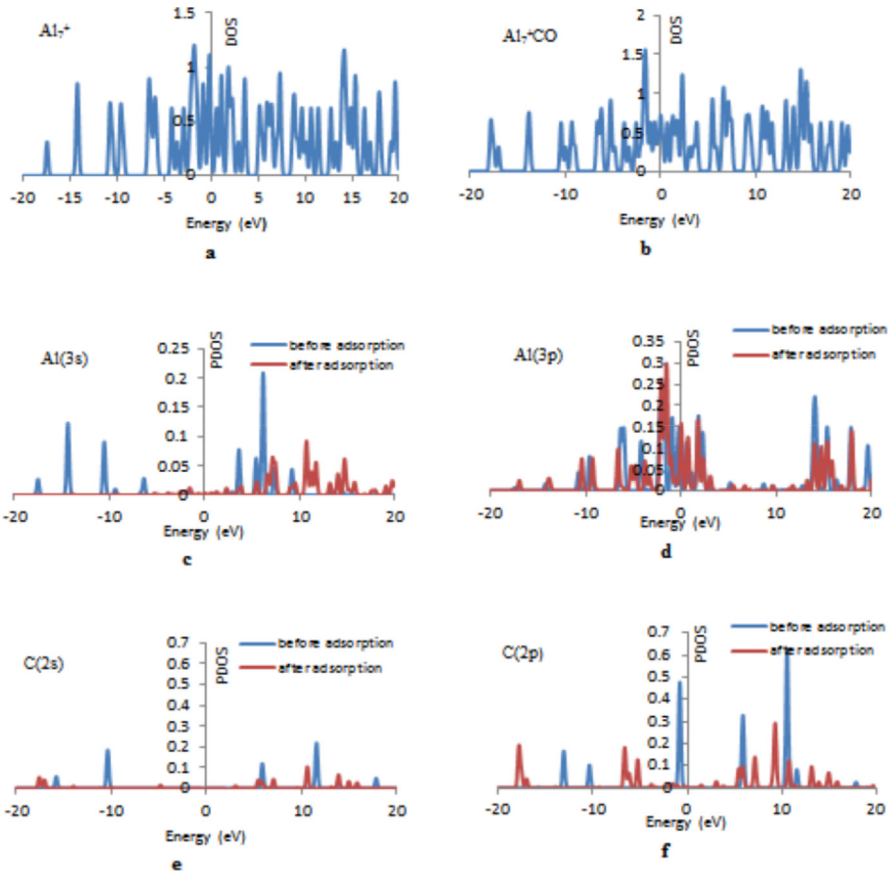

Fig. 17. Total DOS (TDOS) of a) Al_7^+ cluster, b) Al_7^+CO complex (c configuration) as well as partial DOS (PDOS) of c) 3s and d) 3p valence orbitals of Al atom and e) 2s and f) 2p valence orbitals of carbon atom, before and after adsorption.

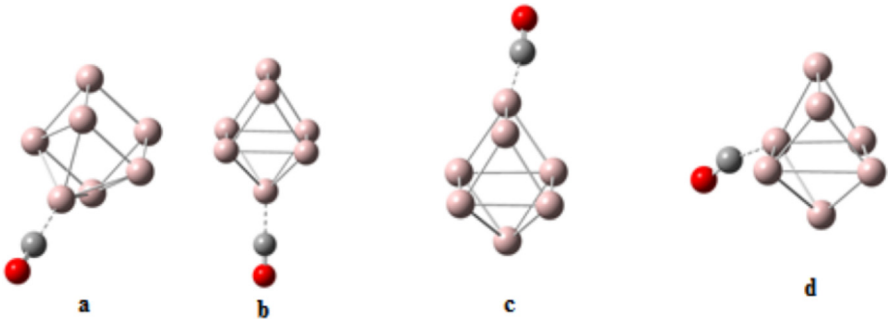

Fig. 18. Optimized structures of Al_7CO complexes in which carbon atom of CO approach to Al_7 from a) below-beside, b) below, c) top and d) top-beside.

bonds (three 3c-2e σ-bonds as well as one 4c-2e σ-bond). All 2c-2e and 4c-2e orbitals are responsible for bonding between the capped aluminum atom and the aluminums of the corresponding face of octahedron. On the other hand, three 3c-2e σ-bonds correspond to three aluminum faces of octahedron. For the π-bonding, the AdNDP analysis reveals three 6c-2e π-bonds and one 7c-2e π-bond involving all aluminum atoms of the cluster. According to this partitioning, Al_7^- possesses 8 delocalized σ and 8 delocalized π electrons, which conform to the 4n Hückel rule for antiaromaticity, for n = 2. Thus, AdNDP anticipates that Al_7^- is both σ- and π-antiaromatic. The double antiaromaticity of Al_7^- cluster justifies its less stability with respect to the Al_7 and Al_7^+.

AdNDP analysis of Al_7^+ reveals ten delocalized bondings consist of three 3c-2eσ, one 4c-2e $\sigma$and three 5c-2e σ-bonds as well as two 6c-2e and one 7c-2e π-bonds (see Fig. 7). It should be mentioned that, the

Table 12
The obtained basis set superposition errors (δ_{BSSE}), deformation (E_{def}), corrected binding (E_{bin}^{corr}), and adsorption energies (E_{ads}^{corr}) as well as H-L gaps for the considered configurations of Al_7^- (all in eV) using B3LYP/6-311G* and Cam-B3LYP/6-311G* [values in bracket] methods.

Configuration	δ_{BSSE}	E_{def}	E_{bin}^{corr}	E_{ads}^{corr}	H-L gap
a	0.0798	0.1607	-0.3300	**-0.1693**	1.5372
	[0.0700]	[0.0952]	[-0.0400]	[0.0552]	[3.3687]
b	0.0798	0.1605	-0.3299	**-0.1693**	1.5374
	[0.0870]	[0.1822]	[-0.2355]	**[-0.0533]**	[3.6379]
c	0.0622	0.1279	-0.1918	-0.0640	1.4653
	[0.0671]	[0.1284]	[-0.1193]	[0.0091]	[3.4994]
d	0.0731	0.0530	0.0816	0.1346	1.4727
	[0.0287]	[0.0004]	[-0.0006]	[-0.0002]	[3.8646]

same AdNDP orbitals were also predicted for the isoelectronic $MgAl_6$ cluster [55]. Based on this partitioning, seven σ-radial AdNDPs are responsible for σ-aromaticity and three π AdNDP orbitals are responsible for π-aromaticity. Therefore, the system should be considered as doubly (σ- and π-) aromatic. These results are in agreement with the previous findings reported by Sun and coworkers [11], and explain the significant stability of this cluster with respect to Al_7^- one. Note that, all AdNDP orbitals have occupation number (ON) values close to the ideal value of 2.000|e|; which validates these chemical bonding representations.

D) Adsorption of CO on Al_7^-, Al_7^+ and Al_7 clusters

In this section, the interaction of carbon monoxide molecule with Al_7^-, Al_7^+ and Al_7 clusters is investigated using both B3LYP/6-311G* and CAM-B3LYP/6-311G* levels of theory. The possibility of adsorption of CO from both carbon and oxygen atoms and on different sites of each cluster (on top of an aluminum atom, bridge and hallow sites) is examined to determine the most favorable adsorption site for each case. It is found that, those configurations in which the CO molecule is on bridge or hallow sites, rearrange to geometries in which the CO is bonded to an Al atom. Therefore, just the configurations that the carbon monoxide is on top of a given aluminum atom, are considered in the rest of this study (see Fig. 8).

The optimized structures of Al_7–CO, Al_7^+CO and Al_7CO in which CO molecule approaches to Al_7^-, Al_7^+ as well as neutral Al_7 clusters from oxygen atom are shown in Figs. 9, 10, and 11. The obtained energies (see Tables 5, 6, and 7) reveal that the considered clusters do not show a tendency for adsorption of CO molecule through its oxygen atom. For instance, calculated deformation energies for those configurations in which CO molecule is approached to Al_7^- cluster through its oxygen atom (Table 5), are nearly zero. Therefore, it seems that Al_7^- cluster and CO molecule undergo no distortion during this interaction. On the other hand, the corrected adsorption energies for these configurations are positive that indicate to repulsive nature of these interactions. These findings reveal no tendency for adsorption of CO through the oxygen atom on Al_7^- cluster. The same behavior is also observed for the other clusters (see Tables 6 and 7). Therefore, just those configurations corresponded to the adsorption of CO from C atom are considered in the rest of this study.

The optimized structures for different configurations of the Al_7–CO are shown in Fig. 12. The evaluated deformation as well as corrected binding and adsorption energies using B3LYP and CAM-B3LYP methods are also collected in Table 8. The obtained results with B3LYP method show that, the three aluminum atoms of the capped face do not show a tendency for the adsorption of CO molecule (**a** configuration with $E_{ads} \cong$ 0.0382 eV); whereas the evaluated negative adsorption energies for **b**, **c** and **d** configurations ($E_{ads} \cong$ -0.3470 eV) reveal the considerable ability of the other Al atoms to adsorb the CO molecule. The calculated deformation energies for these configurations are all about 0.590 eV that indicate a moderate distortion for Al_7^- cluster when CO molecule is approached to it. However, the corrected adsorption energy values of these configurations show that the interaction of CO with this cluster is a physical adsorption, which could be due to a weak van der Walls interaction between the fragments. Therefore, all Al atoms of Al_7^- cluster have the same tendency for adsorbing CO molecule, except three capped face aluminum atoms. Note that, in **d** configuration, the carbon atom of CO is bonded to the capped Al atom of Al_7^- cluster, and this aluminum atom is to some extent pulled out of cluster in the adsorbed structure.

In all **b**, **c** and **d** configurations, the Al–C distance is about 2.03 Å, which is close to the experimental Al–C bond length reported for aluminum carbide (1.955 Å) [56]. This matches our expectation for carbon-metal bonding. The C–O bond length is merely elongated to 1.183 Å from 1.127 Å (evaluated for the isolated CO using the same computational method) during the adsorption process. The structural variation of CO should be related to the electron donation and back-donation between Al atom and CO molecule. It is recalled that, according to the Dewar–Chatt–Duncanson model [57] the CO molecule donates electrons

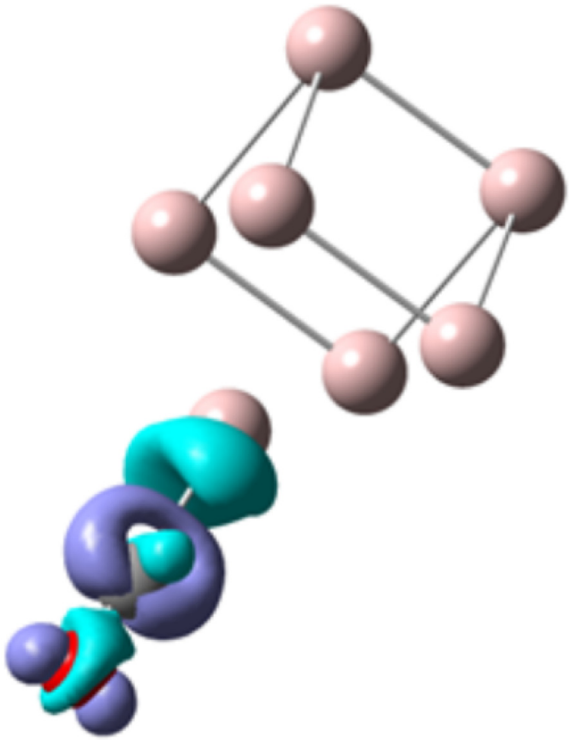

Fig. 19. Difference of electron density of Al_7CO (**a** configuration). The blue and green isosurfaces represent the region in which electron density is increased and decreased, respectively after CO binds to Al_7 (isovalue = 0.005a.u.).

Table 13
Natural charge population of the Al_7CO complex by B3LYP/6-311G* method. The charge values of Al atoms that are bonded to CO are bolded.

	Al1	Al2	Al3	Al4	Al5	Al6	Al7	C	O
Al_7	0.015	0.089	0.089	-0.124	-0.111	-0.112	0.154		
a	0.027	**-0.113**	0.027	0.027	0.026	0.057	0.058	0.282	-0.392
B	**-0.113**	0.026	0.027	0.056	0.027	0.027	0.057	0.282	-0.392
c	0.031	0.063	0.049	-0.019	-0.032	0.027	**0.027**	0.251	-0.397
d	0.016	0.103	0.115	-0.085	**-0.323**	-0.117	0.176	0.491	-0.377

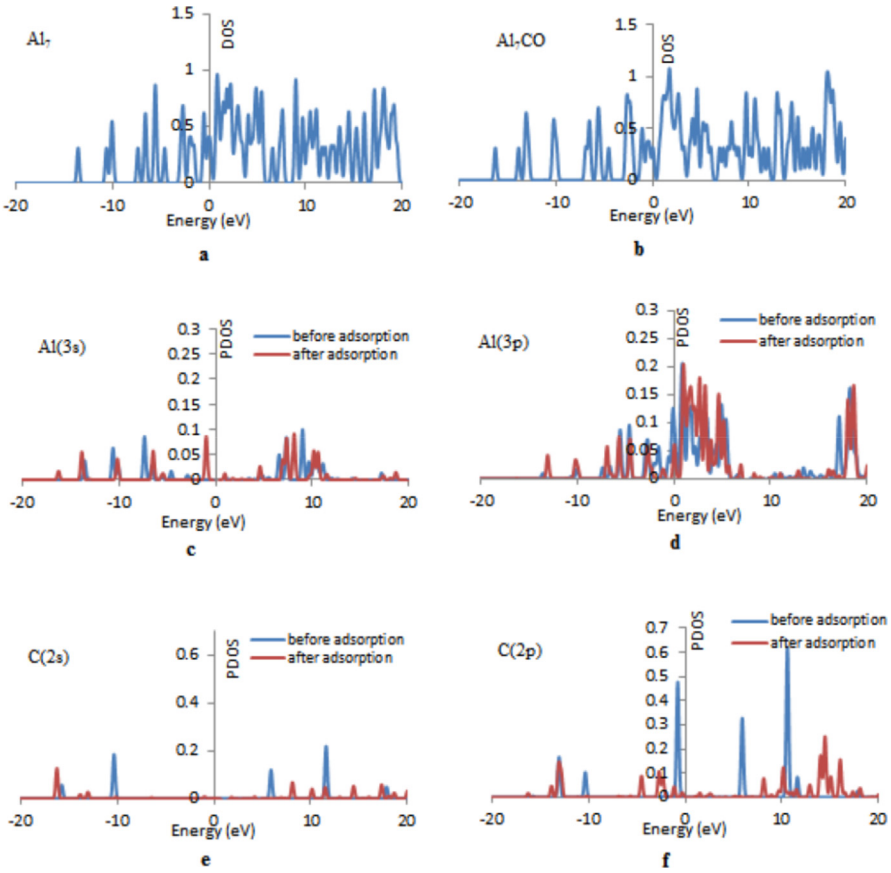

Fig. 20. Total DOS (TDOS) of a) Al_7 cluster, b) Al_7CO complex (**a** configuration) as well as partial DOS (PDOS) of c) 3s and d) 3p valence orbitals of Al atom and e) 2s and f) 2p valence orbitals of carbon atom, before and after adsorption.

from carbon atom into the metal d-orbital and simultaneously the metal donates electrons back from a different filled orbital into the empty π*antibonding orbital of CO. Both of these effects tend to reduce the carbon-oxygen bond order, leading to an elongated C–O distance and a lowering of its vibrational frequency as well as bond strength. But it should be mentioned that, this elongation is not dissociative. The obtained results from CAM-B3LYP calculations are also in the same line (see Table 8).

The Electron density difference (EDD) map can be used to accurately treat the local changes in charge density which occur when the adsorbate-substrate chemical bond is formed. In the considered system (Al_7–CO), EDD reveals how the bonding of the CO molecule affects the electron distribution relative to the isolated CO molecule and the unperturbed aluminum cluster. The EDD isosurface of the **c** configuration, which is obtained by subtracting the SCF densities of the individual CO and aluminum cluster from the entire Al_7–CO complex, is depicted in Fig. 13. The blue and green isosurfaces represent the region in which electron density is increased and decreased after CO binds to cluster. The obtained EDD map reveals an electron density loss near the carbon atom along the Al–C bond, and a considerable electron accumulation in perpendicular antibonding C–O orbital located mainly on C atom; which are in accordance with the Dewar-Chatt-Duncanson model. The EDD also shows that electron back donation from Al to C is more than the reverse charge transfer; which could be due to the negative charge of the aluminum cluster.

The obtained NBO charges for the Al_7–CO complex using B3LYP/6-311G* level of theory are gathered in Table 9. For each configuration the charge value of the Al atom which is bonded to CO molecule is bolded. In this table, charges of aluminum atoms in the isolated Al_7^- cluster are also given for comparison. Although the charge of Al5 atom in the **a** configuration becomes more negative during the complexation (-0.466a.u.), the total charge on CO fragment does not change considerably (–0.034 a.u.). This is in accordance with the repulsive nature of this interaction. On the other hand, the charges of Al1 (in **b** and **c** configurations) and Al7 (in **d** configuration) atoms change to positive values; which imply to decrease of electron density around those atoms during the adsorption of CO molecule. The evaluated considerable negative charge for CO fragment in these interactions (–0.584 a.u.) reveals electron transfer from Al cluster to CO molecule; which confirms the results of EDD analysis. Therefore, it seems that the stability of Al_7–CO should be due to an electron transfer from aluminum cluster to the CO fragment.

The obtained frontier molecular orbitals (HOMO and LUMO) of the Al_7^- cluster using B3LYP/6-311G* are depicted in Fig. 3. The distribution of electron density of these orbitals around the whole aluminum atoms reveals both the electron donor and electron acceptor character of these atoms. Increasing the H-L gap during the complexation with CO (H-L gap changes from 1.59 eV to 1.73eV) indicates that further interaction of CO molecule with this cluster is not favorable.

The partial density of states (PDOS) of free CO and Al_7^- cluster as well as Al_7–CO complex are analyzed to understand the bonding characteristics of CO adsorbed system. The obtained plots are depicted in Fig. 14. There exist new peak around -8.5 eV in the Al_7–CO complex in comparison with the free Al_7^- cluster, stemming from the 3p electron of Al atoms due to the 3s to 3p electron promotion. Additionally, the new peak at -12.5 eV can participate into the orbital overlaps with CO molecule. This results into the physical interaction between CO and Al_7^- cluster.

In **a**′, **b**′ and **c**′ configurations shown in Fig. 10, CO molecule approaches to Al_7^+ cluster through oxygen atom. Calculated deformation energies of those complexes (with B3LYP method) are 0.0024, 0.0029, 0.0036 (in eV) and the evaluated adsorption energies are just -0.0325, -0.0320, -0.0399 (in eV), respectively. Calculated adsorption energies using CAM-B3LYP/6-311G* are to some extent greater than those

evaluated by B3LYP/6-311G* method (see Table 6); but are in the same line. Note that, the calculated adsorption energies for those configurations in which CO approaches to the Al_7^+ cluster from the oxygen atom are negligible.

Fig. 15 shows three different optimized configurations of Al_7^+CO complex in which binding is occurred through C atom. The deformation as well as corrected binding and adsorption energies at B3LYP and CAM-B3LYP are also gathered in Table 10. Note that in B3LYP method, the evaluated deformation (0.0403, 0.0555, 0.0549), adsorption (-0.1087, -0.1455, -0.1459) and binding (-0.1490, -0.2009, -0.2008) energies for the adsorption of CO on Al_7^+ cluster are considerably smaller than the corresponding values for Al_7^- cluster. This implies that there is fewer tendency for adsorbing CO molecule; which could be due to more stability of Al_7^+ cluster resulted from its aromaticity. The similar conclusion is obtained from the CAM-B3LYP calculations (see Table 10).

The Al–C bond lengths in **a**, **b** and **c** configurations are 2.277Å, 2.265 Å and 2.266 Å, respectively; which are longer than the corresponding Al–C bond lengths in Al_7–CO complex (2.029 Å). In these configurations, the C–O bond lengths vary slightly from 1.127 Å (in isolated CO) to 1.122Å (**a**), 1.121 Å (**b**) and 1.121 Å (**c**).Therefore, it seems that CO molecule just undergoes a weak physical adsorption through its carbon atom on Al_7^+ cluster. All of these results indicate to more stability (fewer tendency for CO adsorption) of Al_7^+ cluster with respect to Al_7^-; which is revealed by aforementioned AdNDP analysis.

The calculated H-L gaps for all Al_7^+CO complexes (~2.35 eV) are to some extent less than the H-L gap of the pristine cluster (~2.67 eV). This indicates to decreasing the stability of the system upon the adsorption of CO molecule; which should be due to the loosing of aromaticity. In fact, special stability of Al_7^+ cluster is reflected in its aromaticity and large H-L gap. Electron density difference surface of the **c** configuration for Al_7^+CO is depicted in Fig. 16. The obtained EDD map indicates the increasing electron density along the Al–C bond while near the oxygen atom, electron density is decreased. Indeed the NBO atomic charges of Al_7^+CO complex for **a**, **b** and **c** configurations are gathered in Table 11. The results show that in each configuration the positive charge of Al atom bonded to CO molecule is changed to negative value after adsorption. In these configurations the sum of positive charges of all Al atoms in Al_7^+CO complex is reduced with respect to the bare Al_7^+ cluster; whereas the charge of CO becomes positive after the adsorption. Therefore, NBO results reveal electron transfer from CO molecule to Al_7^+ cluster. Although the DOS plot of Al_7^+ does not alter during the adsorption of CO (see Fig. 17), the appeared peak at -5 eV of Al_7^+CO complex could be participate into the orbital overlaps with CO molecule.

The different optimized structures of Al_7CO (by B3LYP) that binding is occurred from C atom are shown in Fig. 18. The obtained distances between two fragments (Al–C bond length) using B3LYP method in **a**, **b** and **c** configurations are 1.960 Å; which is very close to the Al–C bond length in aluminum carbide (1.955 Å). In these configurations the C–O bond lengths are 1.153 Å, which is to some extent larger than the bond length of free CO (1.127 Å). But for **d** configuration, in which the CO is approached to one of the aluminum atoms of the capped face, the Al–C and C–O bond lengths are 2.180 Å and 1.133 Å, respectively. Therefore, it seems that CO molecule does not prefer these Al atoms for binding.

The evaluated corrected binding, adsorption and deformation energies for Al_7CO using B3LYP and CAM-B3LYP methods are given in Table 12. The obtained results from CAM-B3LYP method show that in a, c and d configurations the neutral Al_7 has no tendency to adsorb CO molecule; whereas negligible negative adsorption energy is predicted for **b** configuration. The obtained results from B3LYP calculation are not in agreement with the CAM-B3LYP results. It should be due to long-range interactions which are important in neutral systems such as Al_7 and CO. Note that for charged systems (like Al_7^+ and Al_7^-), in which the electrostatic contribution is dominant, these effects are negligible and therefore the obtained results from both B3LYP and CAM-B3LYP methods are in the same line.

The Natural Bond Orbital analysis results for different configurations of Al_7CO complex are gathered in Table 13. It is clear that, in each case the bonded aluminum atom becomes more negative with respect to the bare cluster. On the other hand, the charges of CO fragment in stable **a**, **b** and **c** configurations are negative; whereas for **d** configuration a positive value is obtained for carbon monoxide fragment. Therefore, a charge transfer from cluster to the CO molecule is expected in this system. This prediction is confirmed by EDD isosurace of this complex shown in Fig. 19. This figure reveals electron accumulation between the carbon and aluminum atoms, which indicates to an interaction between the fragments.

The partial density of states (PDOS) of free CO molecule and Al_7 cluster as well as Al_7CO complex are shown in Fig. 20. Comparing to the free Al_7 cluster, there exist new peak around -10.7eV in the Al_7CO complex. Although the DOS and PDOS of aluminum atom does not change considerably; s and p electrons of carbon atom with -10.5 eV energies are absent after adsorption. This may show the orbital overlaps between CO molecule and cluster.

4. Conclusion

All the considered Al clusters have octahedral structures with an aluminum atom decorating one of the aluminum faces of the octahedron. AdNDP analysis predicts aromatic and antiaromatic characters (double σ- and π-) for Al_7^+ and Al_7^- clusters, respectively. Al_7^+ has special stability and larger H-L gap as a result of its aromaticity and its electron count (20) matching a shell closing in the Jelllium model. Among the considered aluminum clusters, Al_7^- shows the most tendency for the adsorption of CO molecules, whereas the evaluated smaller adsorption energies of CO on Al_7^+ and Al_7 suggest an inadequate physisorption of carbon monoxide by these clusters. The electronic and structural investigations prove that the adsorption is not dissociative.

Declarations

Author contribution statement

Zeinab Abdeveiszadeh: Performed the experiments; Analyzed and interpreted the data.

Ehsan Shakerzadeh: Analyzed and interpreted the data.

Siamak Noorizadeh: Conceived and designed the experiments; Analyzed and interpreted the data; Wrote the paper.

Funding statement

This work was supported by Shahid Chamran University of Ahvaz, Ahvaz, Iran Grant NO: Grant1396.

Competing interest statement

The authors declare no conflict of interest.

Additional information

No additional information is available for this paper.

References

[1] R. Fournier, Theoretical study of the structure of silver clusters, J. Chem. Phys. 115 (2001) 2165–2177.

[2] J. Wang, G. Wang, J. Zhou, Density-functional study of Au_n(n=2–20) clusters: Lowest-energy structures and electronic properties, Phys. Rev. B 66 (2002) 035418-1–035418-6.

[3] S. Krüger, S. Vent, F. Krüger, M. Staufer, N. Rösch, The average bond length in Pd clusters Pd_n, n=4-309: A density-functional case study on the scaling of cluster properties, J. Chem. Phys. 115 (2001) 2082–2087.

[4] G. Zanti, D. Peeters, DFT Study of small palladium clusters Pd and their interaction with a CO ligand (n= 1-9), Eur. J. Inorg. Chem. (2009) 3904–3911.

[5] H. Ruuska, T.A. Pakkanen, R.L. Rowley, MP2 study on water adsorption on cluster models of Cu(111), J. Phys. Chem. B 108 (2004) 2614–2619.

[6] M. Salazar-Villanueva, J.F. Rivas-Silva, J.I. Rodríguez Mora, J.A. Ascencio, Stable Ti_n ($n = 2–15$) clusters and their geometries: DFT calculations, J. Phys. Chem. A 110 (2006) 10274–10278.

[7] A. Robina, E. Germán, M.E. Pronsato, A. Juan, I. Matolínová, V. Matolin, Electronic structure and bonding of small Pd clusters on stoichiometric and reduced SnO_2(110) surfaces, Vacuum 106 (2014) 86–93.

[8] K. Mašek, P. Blumentrit, J. Beran, I.Píš T. Skála, J. Polášek, V. Matolin, Structural and electronic studies of supported Pt and Au epitaxial clusters on tungsten oxide surface, Vacuum 27 (2012) 586–589.

[9] B.K. Rao, P. Jena, S. Burkart, G. Ganteför, G. Seifert, AlH_3 and Al_2H_6: Magic clusters with unmagical properties, Phys. Rev. Lett. 86 (2001) 629–695.

[10] B.K. Rao, P. Jena, Evolution of the electronic structure and properties of neutral and charged aluminum clusters: A comprehensive analysis, J. Chem. Phys. 111 (1999) 1890–1904.

[11] J. Sun, W.C. Lu, H. Wang, Z.S. Li, C.C. Sun, Theoretical study of Al_n and Al_nO ($n = 2–10$) clusters, J. Phys. Chem. A 110 (2006) 2729–2738.

[12] R. Fournier, Trends in energies and geometric structures of neutral and charged aluminum clusters, J. Chem. Theory Comput. 3 (2007) 921–929.

[13] G.H. Pesleherbe, W.L. Hase, Product energy and angular momentum partitioning in the unimolecular dissociation of aluminum clusters, J. Phys. Chem. A 104 (2000) 10556–10564.

[14] S. Huang, K. Liao, B. Peng, Q. Luo, On the potential of using the Al_7 superatom as an excess electron acceptor to construct materials with excellent nonlinear optical properties, Inorg. Chem. 55 (2016) 4421–4427.

[15] D.E. Bergeron, A.W. CastlemanJr, T. Morisato, S.N. Khanna, Formation of $Al_{13}I$: Evidence for the superhalogen character of Al_{13}, Science 304 (2004) 84–87.

[16] D.E. Bergeron, P.J. Roach, A.W. Castleman, N.O. Jones, J.U. Reveles, S.N. Khanna, Reactions of $Al_nI_x^-$ with methyl iodide: The enhanced stability of Al_7I and the chemical significance of active centers, J. Am. Chem. Soc. 127 (2005) 16048–16053.

[17] M. Brack, Multipole vibrations of small alkali-metal spheres in a semiclassical description, Phys. Rev. B 39 (1989) 3533–3542.

[18] W.D. Knight, K. Clemenger, W.A. deHeer, W.A. Saunders, M.Y. Chou, L. M, M.L. Cohen, Electronic shell structure and abundances of sodium clusters, Phys. Rev. Lett. 5 (1984) 2141–2143.

[19] N.D. Bhaasker, R.P. Frueholz, C.M. Klimeak CM, R.A. Cook, Evidence of electronic shell structure in RbN + (N=1-100) produced in a liquid-metal ion source, Phys. Rev. B 36 (1987) 4418–4421.

[20] H.A. Al-Abadleh, V.H. Grassian, FT-IR study of water adsorption on aluminum oxide surfaces, Langmuir 19 (2003) 341–347.

[21] C. Herdes, Zh Lin, A. Valente, J.A.P. Coutinho, L.F. Vega, Nitrogen and water adsorption in aluminum methylphosphonate α: a molecular simulation study, Langmuir 22 (2006) 3097–3104.

[22] W.M. Sun, Y. Li, D. Wu, Zh Li, Evolution of the structural and electronic properties of beryllium-doped aluminum clusters: comparison with neutral and cationic aluminum clusters, Phys. Chem. Chem. Phys. 14 (2012) 16467–16475.

[23] J.J. Melko, A.W. Castleman, Photoelectron imaging of small aluminum clusters: quantifying s–p hybridization, Phys. Chem. Chem. Phys. 15 (2013) 3173–3178.

[24] R. Shinde, A. Shukla, Large-scale first principles configuration interaction calculations of optical absorption in aluminum clusters, Phys. Chem. Chem. Phys. 16 (2014) 20714–20723.

[25] X-J. Kuang, X-Q. Wang, G-B. Liu, A density functional study on the adsorption of hydrogen molecule onto small copper clusters, J. Chem. Sci. 123 (2011) 743–754.

[26] J.K. Chen, Sh Yang, B.H. Li, Ch Lin, S. Lee, Fluorescence quenching investigation of methyl red adsorption on aluminum-based metal–organic frameworks, Langmuir 34 (2018) 1441–1446.

[27] T. Xu, J.G. Catalano, Impacts of surface site coordination on arsenate adsorption: macroscopic uptake and binding mechanisms on aluminum hydroxide surfaces, Langmuir 32 (2016) 13261–13269.

[28] J.M. Findley, P.I. Ravikovitch, D.S. Sholl, The effect of aluminum short-range ordering on carbon dioxide adsorption in zeolites, J. Phys. Chem. C 122 (2018) 12332–12340.

[29] T. Nakazawa, T. Igarashi, T. Tsuru, Y. Kaji, Ab initio calculations of Fe–Ni clusters, Comput. Mater. Sci. 46 (2009) 367–375.

[30] Q. Ma, Z. Xie, J. Wang, Y. Liu, Y. Li, Structures, binding energies and magnetic moments of small iron clusters: A study based on all-electron DFT, Solid State Commun. 142 (2007) 114–119.

[31] T.H. Upton, D. Cox Man, A. Kaldor, Physics and Chemistry of Small Clusters, Springer, Bostom. USA, 1987.

[32] D.J. Henry, I. Yarovsky, Dissociative adsorption of hydrogen molecule on aluminum clusters: effect of charge and doping, J. Phys. Chem. A 113 (2009) 2565–2571.

[33] M. Maatallah, M. Guo, D. Cherqaoui, A. Jarid, J.F. Liebman, Aluminium clusters for molecular hydrogen storage and the corresponding alanes as fuel alternatives: A structural and energetic analysis, Int. J. Hydrogen Energy 38 (2013) 5758–5767.

[34] P. Shao, X.Y. Kuang, L.P. Ding, M.M. Zhong, Y.R. Zhao, Probing the structural and electronic properties of small aluminum dideuteride clusters, J. Mol. Graph. Model. 53 (2014) 168–178.

[35] H. Cui, G. Zhang, X. Zhang, J. Tang, Rh-doped $MoSe_2$ as a toxic gas scavenger: a first-principles study, Nanoscale Adv 1 (2019) 772–780.

[36] H. Cui, X. Zhang, J. Zhang, M.A. Mehmood, Interaction of CO and CH_4 adsorption with noble metal (Rh, Pd, and Pt)-decorated N_3-CNTs: A first-principles study, ACS Omega 3 (2018) 16892–16898.

[37] H. Cui, D. Chen, Y. Zhang, X. Zhang, Dissolved gas analysis in transformer oil using Pd catalyst decorated $MoSe_2$ monolayer: A first-principles theory, Sustain. Mater. Technol. 20 (2019), e00094.

[38] D. Kumar, S. Krishnamurty, S. Pal, Dissociative adsorption of molecular hydrogen on BN-doped graphene-supported aluminum clusters, J. Phys. Chem. C 121 (2017) 26493–26498.

[39] V.K. Rathore, P. Mondal, Competitive adsorption of arsenic and fluoride onto economically prepared aluminum oxide/hydroxide nanoparticles: Multicomponent isotherms and spent adsorbent management, Ind. Eng. Chem. Res. 56 (2017) 8081–8094.

[40] P.S. Bagus, K.H. Hermann, C.W. Bauschlicher, A new analysis of charge transfer and polarization for ligand–metal bonding: Model studies of Al_4CO and Al_4NH_3, J. Chem. Phys. 80 (1984) 4378–4386.

[41] P.S. Bagus, K. Hermann KH, C.W. Bauschlicher, On the nature of the bonding of lone pair ligands to a transition metal, J. Chem. Phys. 81 (1984) 1966–1974.

[42] M.J. Frisch, G.W. Trucks, H.B. Schlegel, G.E. Scuseria, M.A. Robb, J.R. Cheeseman, G. Scalmani, V. Barone, B. Mennucci, G.A. Petersson, et al., Gaussian 09, Revision A.02, Gaussian, Inc., Wallingford, CT, 2009.

[43] L.F. Cui, X. Li, L.S. Wang, Photoelectron spectroscopy of $Al_nD_2^-$(n=3–15): Observation of chemisorption and physisorption of dideuterium on aluminum cluster anions, J. Chem. Phys. 24 (2006) 054308–054312.

[44] K.H. Ayub, Are phosphide nano-cages better than nitride nano-cages? A kinetic, thermodynamic and non-linear optical properties study of alkali metal encapsulated $X_{12}Y_{12}$ nano-cages, J. Master. Chem. C. 4 (2016) 10919–10934.

[45] Z. Slanina, F. Uhlik, X. Zhao, E. Ōsawa, Enthalpy–entropy interplay for C_{36} cages: B3LYP/6-31G*calculations, J. Chem. Phys. 113 (2000) 4933–4937.

[46] A. Ahmadi, M. Kamfiroozi, J. Beheshtian, N.L. Hadipour, The effect of surface curvature of aluminum nitride nanotubes on the adsorption of NH_3, Struct. Chem. 22 (2011) 1261–1265.

[47] B.G. Willis, K.F. Jensen, An evaluation of density functional theory and ab initio predictions for bridge-bonded aluminum compounds, J. Phys. Chem. A 102 (1998) 2613–2633.

[48] J. Zhang, G. Frenking, Quantum chemical analysis of the chemical bonds in tris(8-hydroxyquinolinato)aluminum as a key emitting material for OLED, J. Phys. Chem. A 108 (2004) 10296–10301.

[49] S.F. Boys, F. Bernardi, The calculation of small molecular interactions by the differences of separate total energies. Some procedures with reduced errors, Mol. Phys. 19 (1970) 553–566.

[50] T. Lu, F. Chen, Multiwfn: a multifunctional wavefunction analyzer, J. Comput. Chem. 33 (2012) 580–592.

[51] R.G. Pearson, The principle of maximum hardness, Acc. Chem. Res. 26 (1993) 250–255.

[52] A.I. Boldyrev, L.S. Wang, All-metal aromaticity and antiaromaticity, Chem. Rev. 105 (2005) 3716–3757.

[53] D.Y. Zubarev, A.I. Boldyrev, Developing paradigms of chemical bonding: adaptive natural density partitioning, Phys. Chem. Chem. Phys. 10 (2008) 5207–5217.

[54] A.P. Sergeeva, A.I. Boldyrev, The chemical bonding of Re_3Cl_9 and revealed by the adaptive natural density partitioning analyses, Commun. Inorg. Chem. 31 (2010) 2–12.

[55] X. Xing, J. Wang, X. Xia, C. Lu, G. Maroulis, Probing the low-energy structures of aluminum–magnesium alloy clusters: a detailed study, Phys. Chem. Chem. Phys. 18 (2016) 26177–26183.

[56] Shen VK, Siderius DW, Krekelberg WP, Hatch HW, NIST Standard Reference Simulation Website, NIST Standard Reference Database Number 173, National Institute Of Standards and Technology, Gaithersburg MD, 20899.

[57] G.J. Leigh, N. Winterton, Modern Coordination Chemistry. The Legacy of Joseph Chatt, Royal Society of Chemistry, London, 2002.